U.S. DEPARTMENT OF ENERGY

PNNL-27065

Prepared for the U.S. Department of Energy
Under Contract DE-AC05-76RL01830

Electron Microscopy Characterization of Suspended Solids from Hanford Tank 241-AP-105 Direct Feed Waste

EC Buck

November 2017

Pacific Northwest
NATIONAL LABORATORY

DISCLAIMER

PACIFIC NORTHWEST NATIONAL LABORATORY
operated by
BATTELLE
for the
UNITED STATES DEPARTMENT OF ENERGY
under Contract DE-AC05-76RL01830

Printed in the United States of America

Available to DOE and DOE contractors from the
Office of Scientific and Technical Information,
P.O. Box 62, Oak Ridge, TN 37831-0062;
ph: (865) 576-8401
fax: (865) 576-5728
email: reports@adonis.osti.gov

Available to the public from the National Technical Information Service
5301 Shawnee Rd., Alexandria, VA 22312
ph: (800) 553-NTIS (6847)
email: orders@ntis.gov <http://www.ntis.gov/about/form.aspx>
Online ordering: http://www.ntis.gov

Electron Microscopy Characterization of Suspended Solids from Hanford Tank 241-AP-105 Direct Feed Waste

EC Buck

November 2017

Pacific Northwest National Laboratory
Richland, Washington 99352

Abstract

The focus of this study is the residual wastes that remained in a liquid Hanford Tank Waste specimen, designated, AP-105. The objective of this work is to determine the nature of the residual wastes, including composition and the possible identification of phases.
There were many iron-rich phases in the waste together with sodium salt phases. The iron-rich phases appeared to be Fe-Cr-Ni steel derived particles. Al-silicates were found and a wispy Cr oxide phase. Boehmite was also identified in the waste. There was evidence for the attachment of Si around the boehmite particles. Boehmite phases were found in close association with Cr-phases but iron was not co-located in these instances.

Acronyms and Abbreviations

DFLAW	Direct Feed Low Activity Waste
EDS	X-ray Energy Dispersive Spectroscopy
keV	kilo-electron volt
PNNL	Pacific Northwest National Laboratory
SEM	Scanning Electron Microscopy
STEM	Scanning Transmission Electron Microscopy
TEM	Transmission Electron Microscopy
wt. %	weight percent
μm	micrometer
WTP	Waste Treatment Plant
XRD	X-ray diffraction

Contents

Figures

Introduction

The March 2016 modification to the Hanford Consent Decree placed a priority on completing those facilities necessary for the vitrification of low-level tank wastes by 2020. This has raised the importance of the Direct Feed Low-Activity Waste (DFLAW) facilities. The Hanford Site tank waste mission is currently focused on completion of DFLAW and the initial waste processing. Completion of the DFLAW process includes (but is not limited to) parameterization of operational conditions associated with filtration, ion exchange, and gas generation in DFLAW and erosion/ corrosion of transfer lines and vessels. The DFLAW flowsheet team is determining ways to minimize liquid salt returns to the tank farms and identify pathways for secondary waste disposal from the evaporator bottoms and wastes related to ion exchange eluate.

As of 1994, the waste in Tank 241-AP-105 (referred to as AP-105 in this report) contained 821,000 gallons of double-shell feed and was 60.6% water with the remainder being dissolved salts. The waste did not contain any solids. The tank was originally placed into service in August 1986 with the addition of flush water. Subsequent additions included evaporator wastes, and wastes transferred from other Hanford tanks. The final transfer of wastes to AP-105 occurred in July 1989 with waste solutions from Tank 241-AP-106. AP-105 was sampled in March 1993 for chemical analysis and the results were reported by DeLorenzo et al. (Report Tank Characterization Report for Double-Shell Tank 241-AP-105, WHC-SD-WM-ER-36- REV 0, September 1994). However, more recent analyses by Ferriter (2016) provide a more accurate analysis of the wastes.

Following operations for treating a waste sample from AP-105, a very small quantity of solid material was retrieved. This material was isolated for further analysis. In this report, the scanning electron microscopy (SEM) characterization is detailed. The objective of the SEM characterization was to determine the particle sizes, compositions and phases of a liquid waste being tested for the DFLAW. The report provides images and x-ray energy dispersive spectra and elemental maps from particles and aggregates analyzed. Quantitative analysis of each analyzed point is reported. The report provides images and x-ray energy dispersive spectra and elemental maps from particles and aggregates analyzed. In some cases semi-quantitative analyses are reported. Although oxygen, carbon, and nitrogen are detectable with EDS, any

quantitative analysis of these is highly erroneous because of low x-ray fluorescence yields, self-absorption, and detector efficiency. Samples were prepared by depositing the solids onto a sticky carbon SEM stub. The stub was not carbon coated and analyses were performed using low vacuum (i.e. small H_2O partial pressure) conditions. The specimen was examined in a FEI (Hillsboro, OR, USA) Quanta 250 FEG (Field Emission Gun) Scanning Electron Microscope equipped with a solid state Peltier-Cooled Silicon Drifted Detectors (SDD) x-ray detector. The x-ray analysis software was EDAX Genesis V.

1.0 Experimental Procedure

The technical or operating procedure (RPL-EMO-1 Rev1) was utilized by this project were reviewed and approved by the Radiochemical Processing Laboratory (RPL) Independent Review Committee (IRC) and appropriate laboratory safety organizations. This process outlines the specific hazards and appropriate mitigating and emergency actions to be followed.

1.1 Micro-structural Analysis of Samples

For SEM, a small quantity of the solid material was placed on a sticky carbon tape mounted on an aluminum SEM stub. The SEM sample was examined in a FEI Quanta250 Field Emission Gun (FEG) equipped with a backscattered electron (BSE) detector and EDAX Genesis x-ray energy dispersive spectrometer (EDS) system in the 325 Building. No conductive carbon coat was used for sample preparation and the instrument was operated in the low-vacuum mode. This enabled analysis of the light element content in the phases. It is not possible to extract quantitative data or even semi-quantitative data on the light elements, but the analysis can confirm their presence. Examples include the identification of $NaNO_3$ and the carbonate mineral, Trona.

1.2 Magnification Scale

Most SEM images were obtained at 15 keV with backscattered imaging to enable the high Z phases to be easily viewed. As the sample was not a polished flat section, it is unreliable to extract quantitative data from the EDS analyses; however, semi-quantitative analysis is reported. Analyses where the lower energy x-rays were present were deleted from consideration.

The SEM magnification scale was calibrated with a National Institute for Science and Technology (NIST) traceable standard. The SEM images of this measurement standard are shown in Figure 1.2. The instrument indicated magnification was within 1% of the expected value. The energy scale was checked by looking at high and low energy x-rays from known materials.

For SEM, a small quantity of the solid material was placed on a sticky carbon tape mounted on an aluminum SEM stub. The SEM sample was examined in a FEI Quanta250 Field Emission

Gun (FEG) equipped with a backscattered electron (BSE) detector and EDAX Genesis x-ray energy dispersive spectrometer (EDS) system in the RPL.

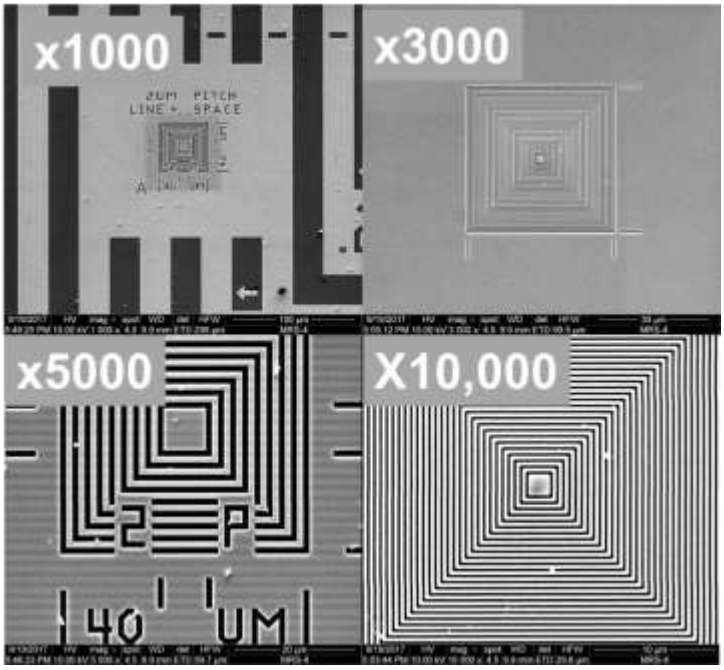

Figure 1-1 SEM images of the magnification standard (MRS-4) showing calibration checked at x1000, x3000, x5000, and x10000 (Taken 09-2017)

1.3 X-ray energy dispersive spectroscopy

The EDS system was calibrated with known compounds. The energy positions of peaks measured on the EDS system have been compared to literature values. The agreement between literature and experimental values was excellent, demonstrating that the system is calibrated correctly for analyzing characteristic x-rays at both low and high energies. The error in the peak energy assignments was estimated to be ~1%. Although AP-105 was a highly radioactive material, it did not create any problems for the EDS system.

2.0 241-AP-105 Residues

According to the report by DeLorenzo et al.,[1] the elements present in the highest concentrations in solution AP-105 waste sample were sodium (1.63×10^8 µg/L), aluminum (4.81×10^6 µg/L), potassium (2.72×10^7 µg/L), silicon (1.45×10^5 µg/g), Mg (9.09×10^3 µg/L), iron (9.61×10^3 µg/L), and chromium (2.67×10^3 µg/L) together with the major anions nitrate (1.59×10^8 µg/L) and carbonate (1.53×10^7 µg/L). Mn and Ni were not reported in the analyses although these were found in the SEM analyses. Phosphorus was reported in the solution and observed in the SEM but has been left out from the analysis below. The concentrations reported by Ferriter et al. (2016) compared to those obtained from EDS analysis of a collection of agglomerates in AP-105 (see Figure 2-1). The major difference in the composition was related to the potassium concentration that was more or less absent in the solids. The initial ^{137}Cs content was measured at 2.73×10^5 µCi/L in March 1994 (calculated activity today would be 1.57×10^5). The major elements reported in the solutions was used as a basis for examining the possible phases that might be present in the residual solid observed.

Figure 2-1 Solution analysis ($\log_e$ µg/L concentration) from Ferriter (2016) and semi-quantitative EDS analysis ($\log_e$ wt%) from this study

The DeLorenzo et al. (1994) reported found no evidence of any solids in the waste material. The solids extracted in this investigation that possessed a high surface area (see Figure 2-2) were extremely low relative to the volume of waste solution processed. The residual consisted of particles generally had three to four common compositions. Sodium nitrate, sodium carbonate, Al-silicate, and iron-chromium phases were also identified in the specimen. The iron-chromium particles appeared to be particles of steel. Boehmite (AlOOH), hematite (Fe_2O_3), and chromium

oxides were also expected to be observed. Several other phases were located with SEM-EDS but definitive phase identification was only possible in a few cases. In Table 2.1, spot semi-quantitative analyses of particles in the wastes are tabulated.

A **B**

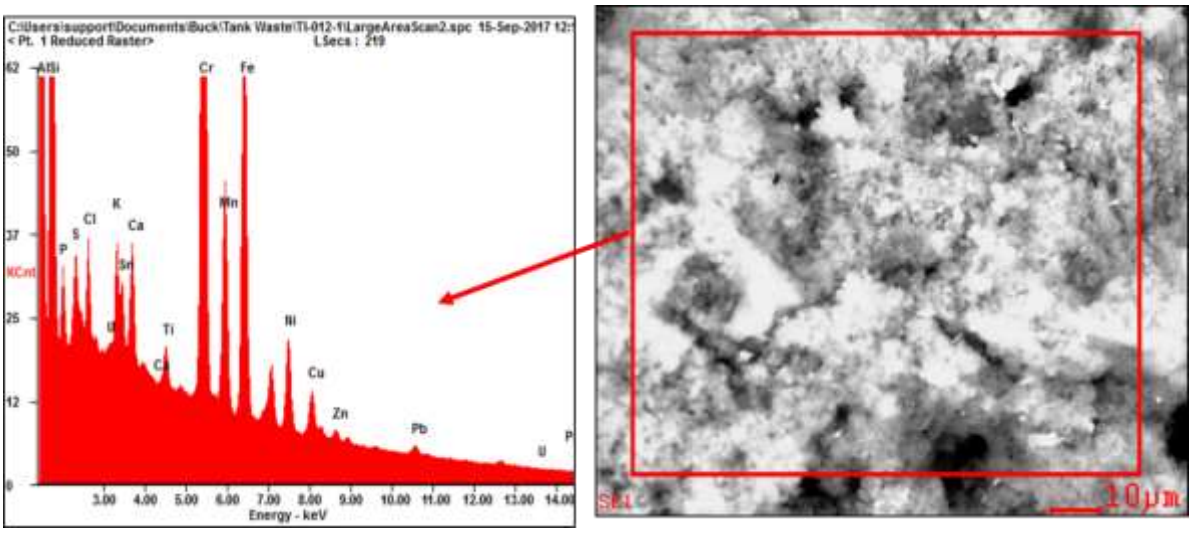

Figure 2-2 (A) EDS Analysis of a large area region shown in (B) which provided an overall composition of the waste solid

Table 2.1 Compositional Analysis of Particles[(a)] in Element (wt%) and Shown in Figure 2-7

Spectrum	1	2	3	4	5	6
NaK	25.58	31.62	33.36	35.18	30.10	28.25
MgK	2.54	3.86	2.29	4.28	3.14	3.11
AlK	17.16	9.20	13.25	18.32	24.74	20.87
SiK	13.82	10.64	7.52	13.71	14.78	16.94
SK	1.65	1.14	1.16	2.32	2.84	1.44
ClK	1.64	0.39	0.60	1.35	1.51	0.39
KK	1.12	0.35	0.61	1.49	1.55	0.32
TiK	1.89	<0.1	<0.1	0.48	0.44	<0.1
CrK	26.36	10.46	4.24	12.27	11.63	9.01
FeK	6.57	27.00	35.95	6.71	6.48	16.61
NiK	1.18	4.98	0.70	2.10	1.82	2.52
CuK	0.49	0.38	0.32	1.79	0.97	0.54

(a) =Concentrations based on compositions (wt%) normalized to 100%. Concentrations listed as "<0.1" indicate that the corresponding element not quantifiable.
(b) Carbon, nitrogen, and oxygen concentrations are suspect and are not reported here.

In Figure 2-3 Example SEM-BSE images showing the types of agglomerate phases in the waste. The image shows that the agglomerates were made of many small particles. The EDS analysis results are shown in Table 2.1. SEM analysis of a group of particles is shown. The contrast was adjusted so that the as many particles as possible were clearly visible. Particle 3 had a high C and O content and may be a carbonate phase and the N-peak is also visible. The EDS results were normalized without the light elements included. Elemental mapping of the specimen at a similar magnification revealed the heterogeneous nature of the material. In Figure 2-4, the distribution of Fe and Al occurs as discrete particles in the solid; whereas, the distribution of chromium was very uniform. The distribution of sodium was also uniform but this is most likely the result of dissolved material precipitating over the sample during drying. It is still noteworthy, the potassium was not observed at similar levels, as this element was identified in the chemical analysis performed during the initial sampling of this waste.

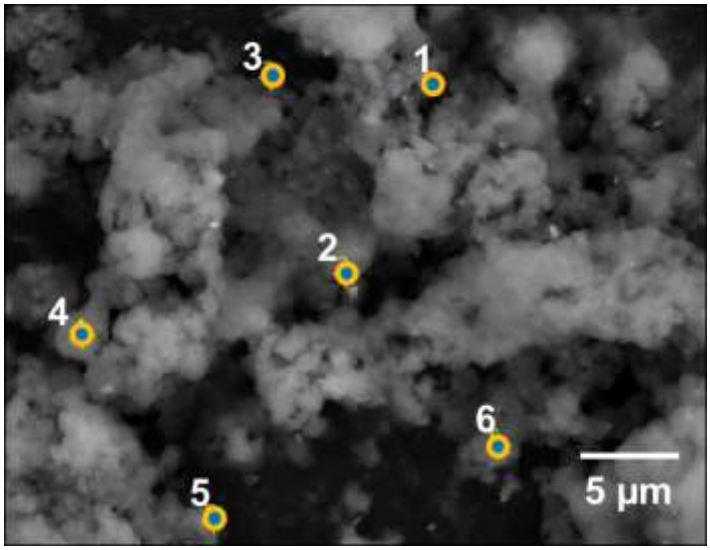

Figure 2-3 Example SEM-BSE images showing the types of agglomerate phases in the waste. The image shows that the agglomerates were made of many small particles. The EDS analysis results are shown in Table 2.1.

Similar spot analyses are shown in Figure 2-5 and selected analyses reported in Table 2.2. In this instance, the reported values for the light elements were included. These are not quantitative results but provide some idea of the level of these light elements in the solid residues.

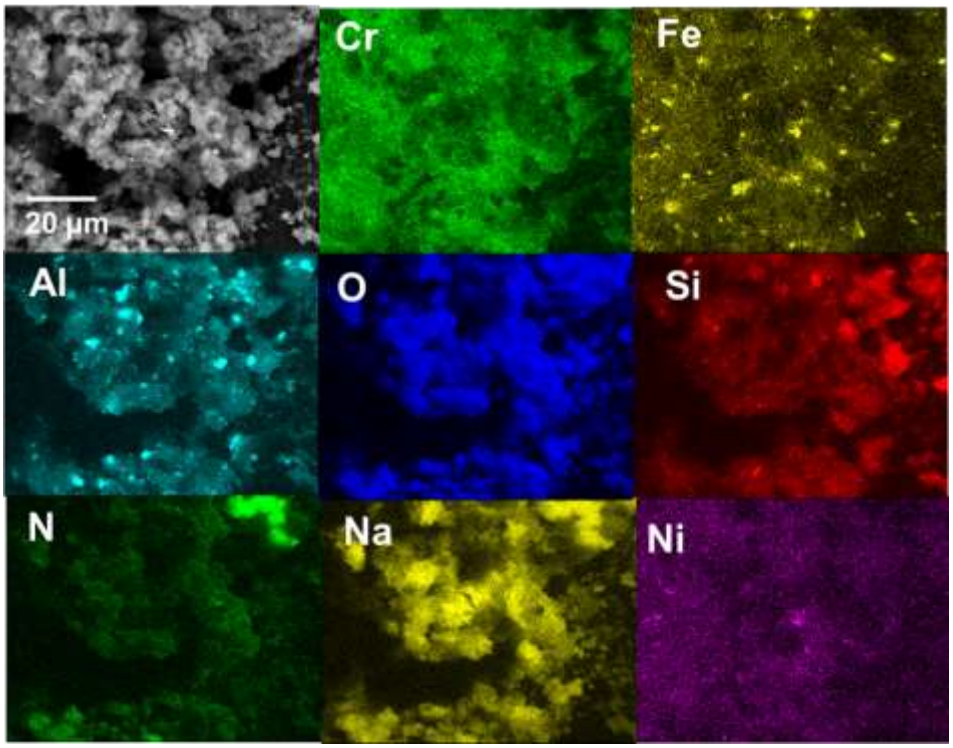

Figure 2-4 Low magnification elemental maps showing major elements and a BSE image of the waste sample.

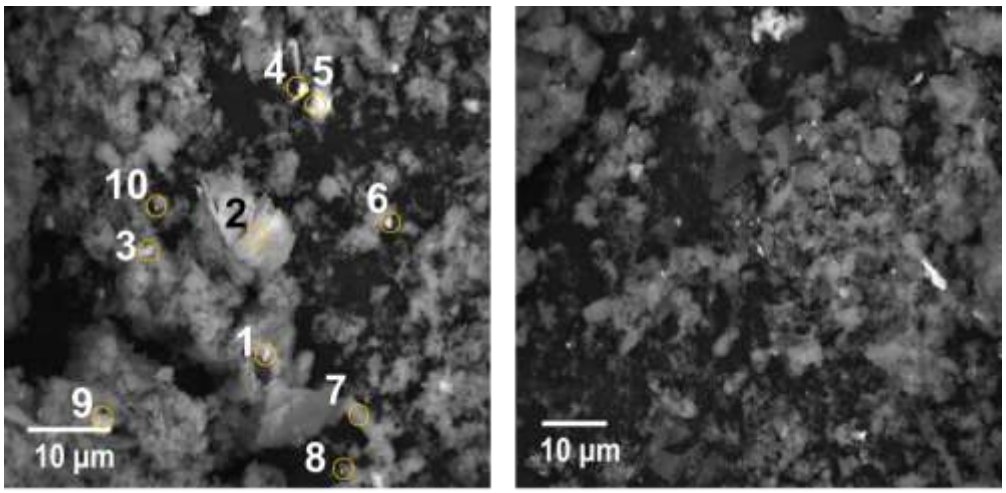

Figure 2-5 (A) SEM-BSE images of the AP-105 tank waste sample showing the presence of a fan-like phase (2)

Table 2.2 Elemental Analysis of particles from AP-105

Region	**1**	**2**	**3**	**5**	**7**	**9**
NaK	26.59	16.46	7.12	6.75	8.05	21.11
MgK	4.24	8.31	0.92	1.20	1.62	4.51
AlK	17.20	10.47	3.10	3.40	4.91	17.32

SiK	19.92	25.54	3.77	4.25	5.66	23.14
CrK	15.08	8.31	2.03	15.99	15.53	22.09
MnK	0.61	20.84	0.37	1.16	1.31	0.52
FeK	13.79	8.73	82.23	59.83	53.62	8.43
NiK	2.58	1.35	0.46	7.41	9.31	2.88

In Figure 2-6, an SEM images and spot analyses of specific regions are shown. In both locations, a high concentration of iron was observed. In one case, there was titanium associated with the particle analyzed. Other particles in this region contained Ag-Hg which has been observed in other Hanford tank waste specimens. A tungsten particle was found and shown in Figure 2-7, although this was rare and the only one found in this instance.

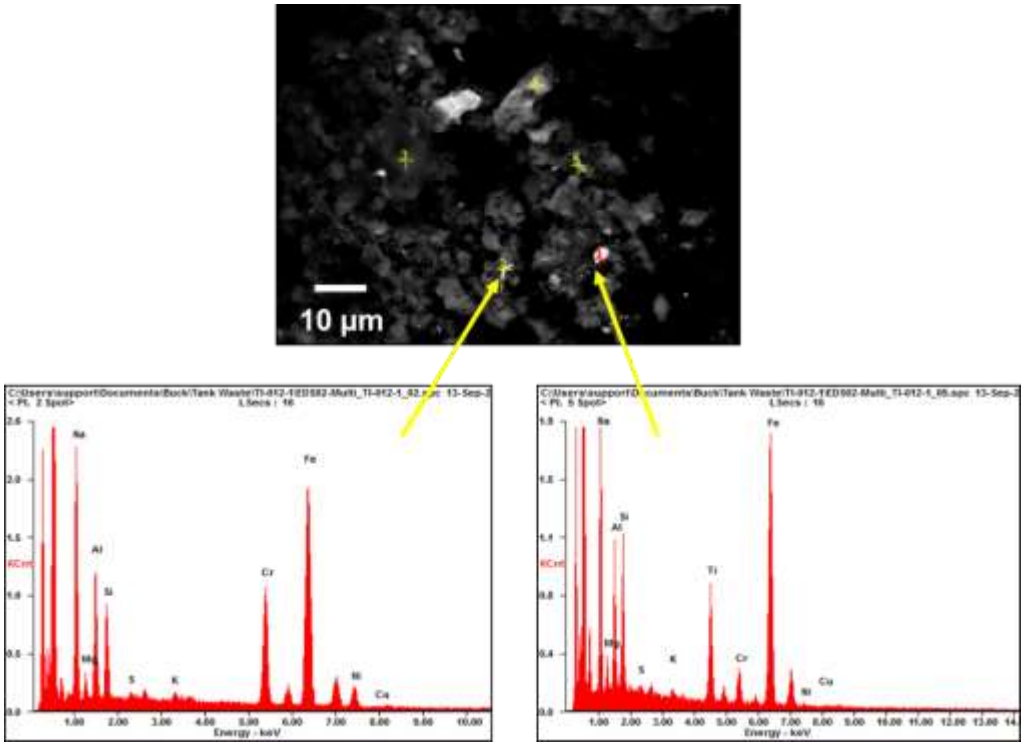

Figure 2-6 SEM image and EDS analysis of agglomerate containing numerous uranium-bearing particles, Al-silicate, and a Ag-Hg containing particle.

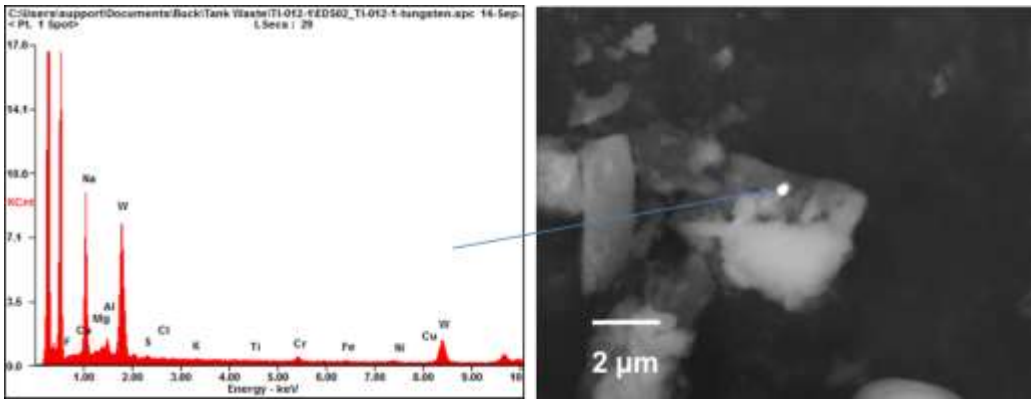

Figure 2-7 EDS analysis and BSE image of W-bearing particle in the AP-105 waste.

The W-bearing particle shown in Figure 2-7 was attached to other light phases. Particles such as those that are W-bearing are extremely bright under BSE imaging and easily found during the analysis.

Table 2.3 Compositional Analysis of Particles in AP-105

Element	**1**	**2**	**3**
Na-K	26.12	41.05	32.42
Mg-K	4.17	2.73	1.55
Al-K	16.89	6.61	45.14
Si-K	19.57	7.66	5.58
S-K	<0.1	<0.1	<0.1
Cl-K	1.41	1.68	1.19
K-K	1.86	0.82	<0.1
Sn-L	1.64	<0.1	<0.1
Ca-K	<0.1	<0.1	<0.1
Ti-K	<0.1	<0.1	9.46
Cr-K	14.81	12.29	4.65
Mn-K	0.00	0.75	<0.1
Fe-K	13.54	26.41	<0.1

In Table 2.3, data from a series of points from Figure 2-8 are reported. For one series of points only a limited number of elements are reported. Mercury and nickel contents are reported in a few spectra. The Mn level in the iron particles was high on occasions. Mn was not reported in the AP-105 sample analysis conducted by DeLorenzo et al. (1994)

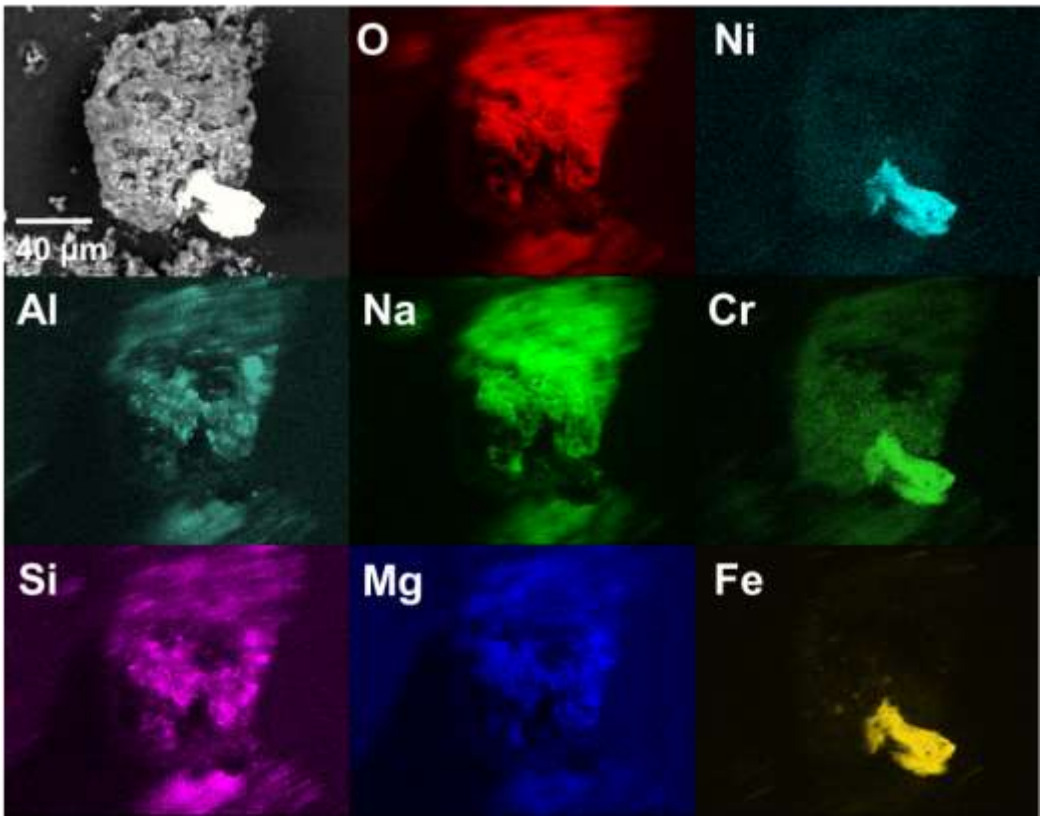

Figure 2-8 Low magnification elemental maps showing major elements and a BSE image of the waste sample. BSE Image of sodium-rich phase and protruding iron-chromium particle in tank waste

The elemental maps in Figure 2-8 and Figure 2-10 show particles rich in Fe and Cr, possibly a steel degradation product. There was no evidence of oxygen in this phase. Mn was rarely observed in the sample; however in Figure 2-9, SEM-BSE and EDS show a Mn-rich particle in the waste. Note that most of the particles in this image are sub-micron. Small particles containing Sn were also observed in the tank waste specimen.

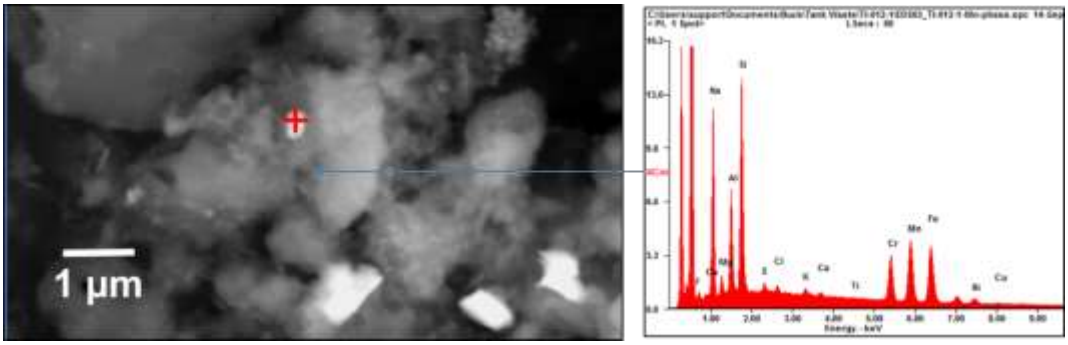

Figure 2-9 BSE image of sub-micron Mn-bearing particle and EDS analysis of the phase

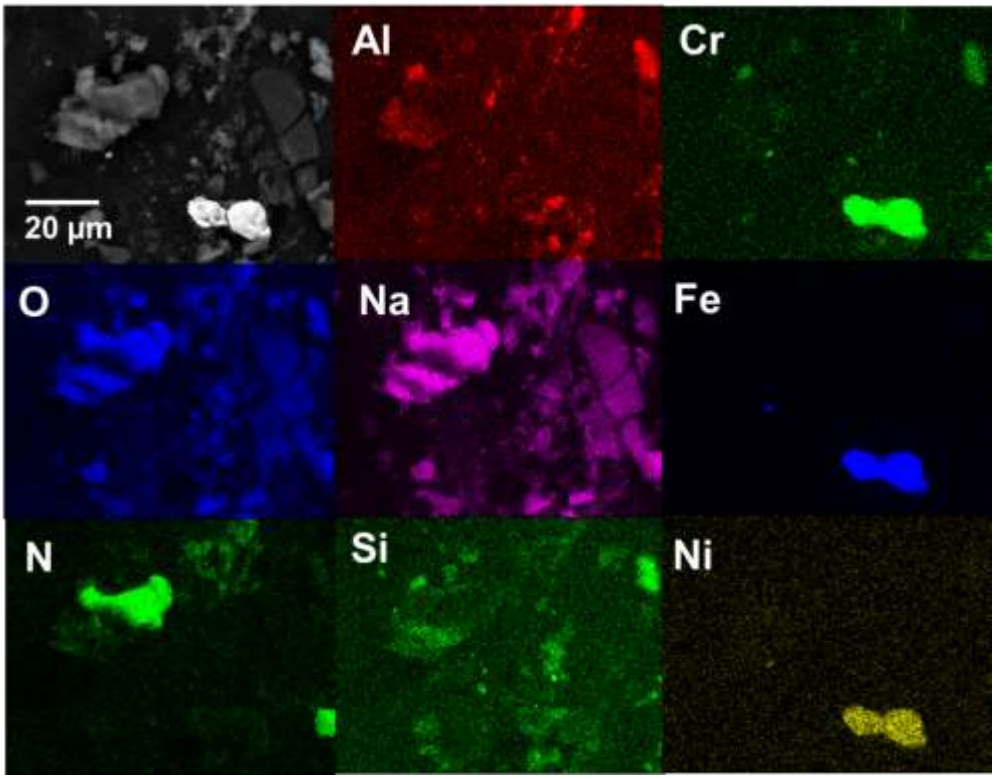

Figure 2-10 Elemental map of AP-105 showing several different phases. The steel-like particle did not contain any oxygen.

In Figure 2-10, the brightest particle is an Fe-Cr particle, possible some form of steel particle as Ni was also detected. The light element maps are unreliable as their characteristic x-rays are easily attenuated by the solids. However, N does show up in agreement with the presence of nitrate solids, most likely NaNO3. This phase has been noted in many Tank waste samples. In the upper right corner of the image, a phase containing Na, Al and Si can be seen. This is likely to be a cancrinite-type phase. Throughout the sample Cr, Si, and Al were found. The exact phase that these were associated with is unknown.

Table 2.4 Compositional Analysis of Selected Particles in AP-105 (Element wt. %) from regions shown in Figure 2-4

Spectrum	1	2	3	4	5
NaK	23.90	22.62	23.17	64.09	11.56
MgK	2.66	2.05	2.26	1.46	0.99
AlK	8.29	7.59	8.78	13.30	2.47
SiK	7.81	6.95	5.76	6.27	2.06
SK	0.50	0.98	0.41	1.14	0.30
KK	0.53	0.77	0.60	1.31	0.39
CrK	9.19	13.63	13.08	6.79	2.36
FeK	4.02	38.74	39.55	3.97	78.74
NiK	42.12	5.98	5.67	1.02	0.61
CuK	0.60	0.68	0.71	.65	0.52

The sodium content in many of the regions analyzed were >20 wt.%. The analysis points represented in Table 2.4 may consist of several phases which explains the occurrence of a large number of elements. The analysis points are shown in Figure 2-11 and, similarly, data from Table 2.5 was extracted from the regions shown.

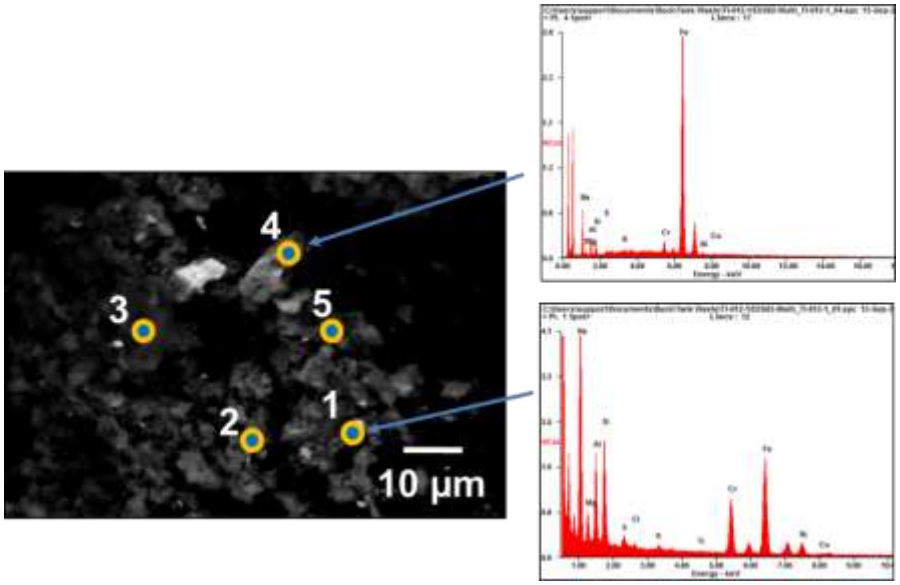

Figure 2-11 Backscattered Electron (BSE) Micrograph and EDS Spectra for Selected Particles Present in the Waste (see Table 2.4).

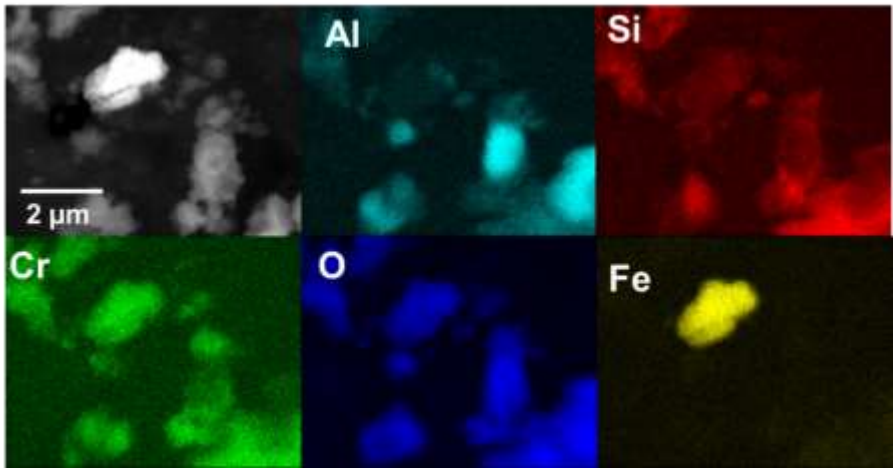

Figure 2-12 Elemental map showing Al-bearing boehmite and surrounding Cr phases and the occurrence of a Fe-Cr particle which did appear to contain oxygen.

Another elemental map (see Figure 2-12) taken at medium magnification shows the distribution of the major elements and in Higher resolution techniques such as TEM/STEM are necessary to determine the exact nature of phases and their possible structures or related structures.

Table 2.5 Compositional Analysis of Selected Particles in AP-105 (wt. %)

Spectrum	**1**	**2**	**3**	**4**	**5**	**6**	**7**	**8**
NaK	19.14	20.21	14.73	5.76	4.64	9.35	8.49	9.49
AlK	4.15	3.66	6.61	12.99	7.05	11.09	12.08	20.74
SiK	2.33	2.97	3.32	4.04	4.91	4.50	7.79	13.87
CaK	3.02	2.74	2.64	3.30	4.23	3.29	3.18	1.72
CrK	1.63	0.51	1.89	6.21	8.13	3.48	4.55	2.58
FeK	9.22	4.82	12.77	42.03	32.16	27.67	30.48	11.38

In Table 2.5Table 2.5, another example of point analyses from different regions in the AP-105 sample is shown. In general, high Na and Fe content was observed throughout the specimen.

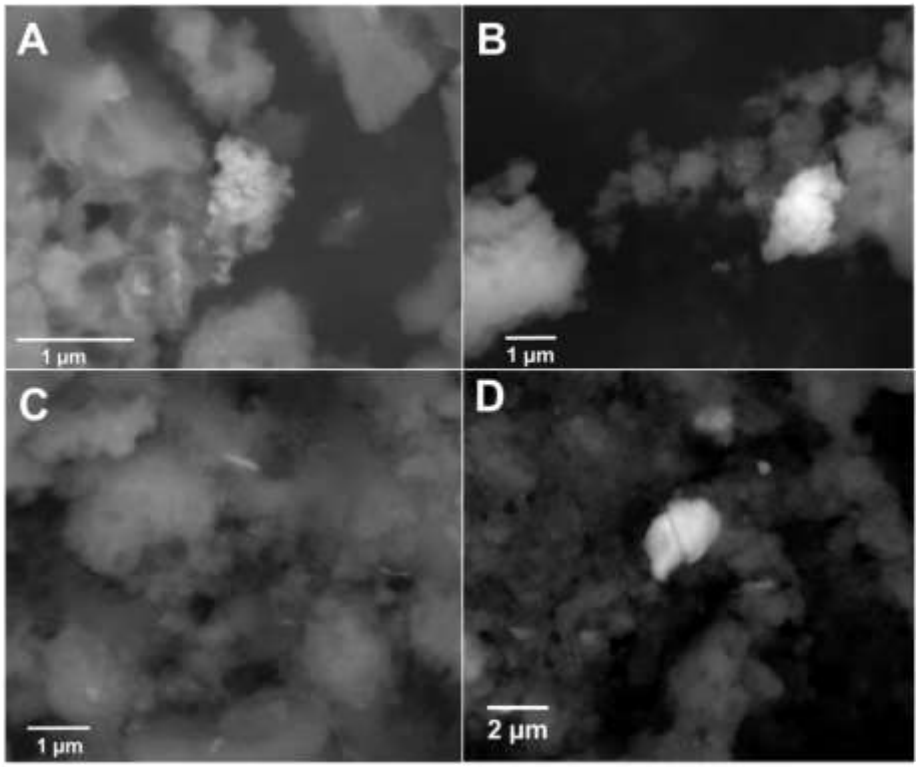

Figure 2-13 Series of four images showing the very small particle size in AP-105

In Figure 2-13, a series of SEM images taken at high magnification show the extremely small particle size range of the material in the waste. In (A), a bright agglomerate is observable that is clearly made from many aggregated particles, all <100 nm. In (B), the characteristic rhombohedral boehmite particles can be seen in the center surrounded by diffuse phases that are of lesser dimensions. In (C), a thin- Fe-rich phase is attached to other very wispy and ill-defined solid materials. These are clearly not salt deposits which tend to have a flat appearance but other types of oxide phases. In (D) a larger particle of iron can be seen but even this larger phase is <5 µm in diameter. In the Discussion Section, particle size analysis of some of these phases is shown.

3.0 Boehmite

The dissolution and precipitation of the aluminum oxy-hydroxide phases, gibbsite [α-$Al(OH)_3$] and boehmite [α-AlOOH] is of prime importance to the final disposition of the caustic high-level nuclear waste (HLW) stored at the Hanford Site. Although, DFLAW involves direct-feeding of wastes to a melter which means the presence of any specific aluminum phases is of little consequence. Nevertheless, the high aluminum content generally in the Hanford Tank waste stream is incompatible with durable glass formulations and, for many other wastes, the Al-content needs to be minimized prior to vitrification. Caustic leaching is performed as part of the WTP at Hanford to handle the high Al content of the wastes. During the examination of the AP-105, small particles of boehmite were observed. Because of the interest in boehmite for many other sludge-based waste tanks, an effort was made to extract as much information from these boehmite particles in AP-105. However, because AP-105 is a liquid-based (extremely low solid content) waste for DFLAW, the occurrence of boehmite is of little impact to waste processing. The only interest in examining the phase is its relevance to other tanks where it is a dominant phase.

Boehmite is orthorhombic (**a** = 0.0285 nm, **b** = 0.1224 nm and **c** = 0.0365 nm). The crystals are typically tabular with the major surfaces normal to **B**<0l0> . In Figure 3-1, an elemental map taken at high magnification shows several small particles including a rhombohedral-shaped Al-particle which is boehmite and a diffuse Cr and Si region. All the materials are oxide, so O shows up on all solids. There was no Fe in the vicinity of this image at least at a significant concentration to be detected.

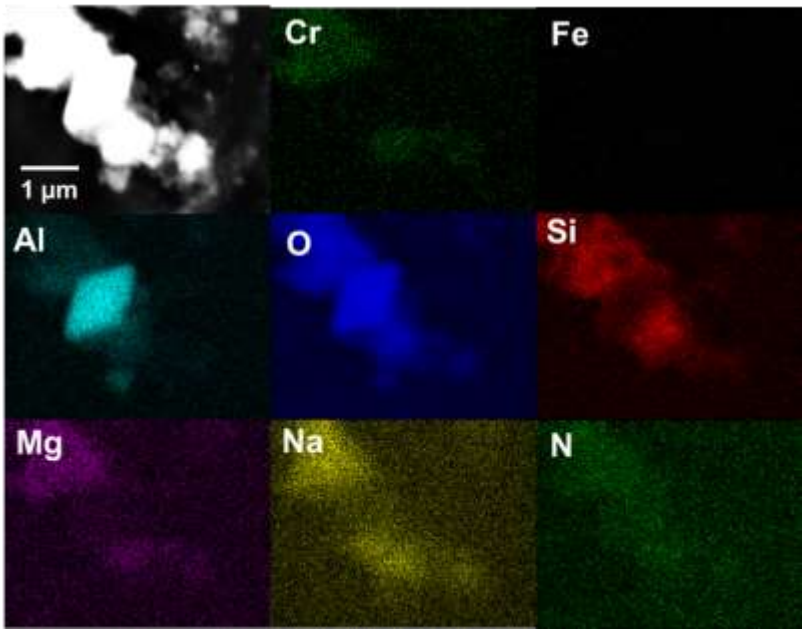

Figure 3-1 High magnification elemental maps of a boehmite particle showing major elements and a BSE image of the waste sample.

One interesting observation was the outlining of the boehmite particle with Si. Although Si is common throughout the sampled region, it appeared to trace around the (101) planes of the boehmite crystal. Direct elemental analysis and imaging of a boehmite particle is shown in Figure 3-2 and this shows the occurrence of both Si and Na in the boehmite phase. Without more detailed analysis with TEM/STEM, it is not possible to determine how these elements are exactly associated with the boehmite particle. A lower magnification elemental map enclosing the same region is shown in Figure 3-3. In this case, the bright particle was found to be an iron-chromium particle similar to those found throughout the solid waste sample. The close association of Cr with the Al was always apparent.

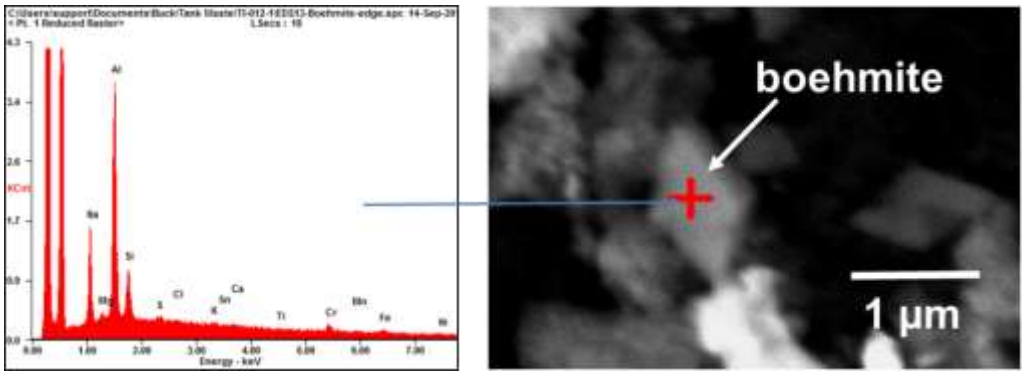

Figure 3-2 EDS analysis and BSE image of boehmite phase in AP-105

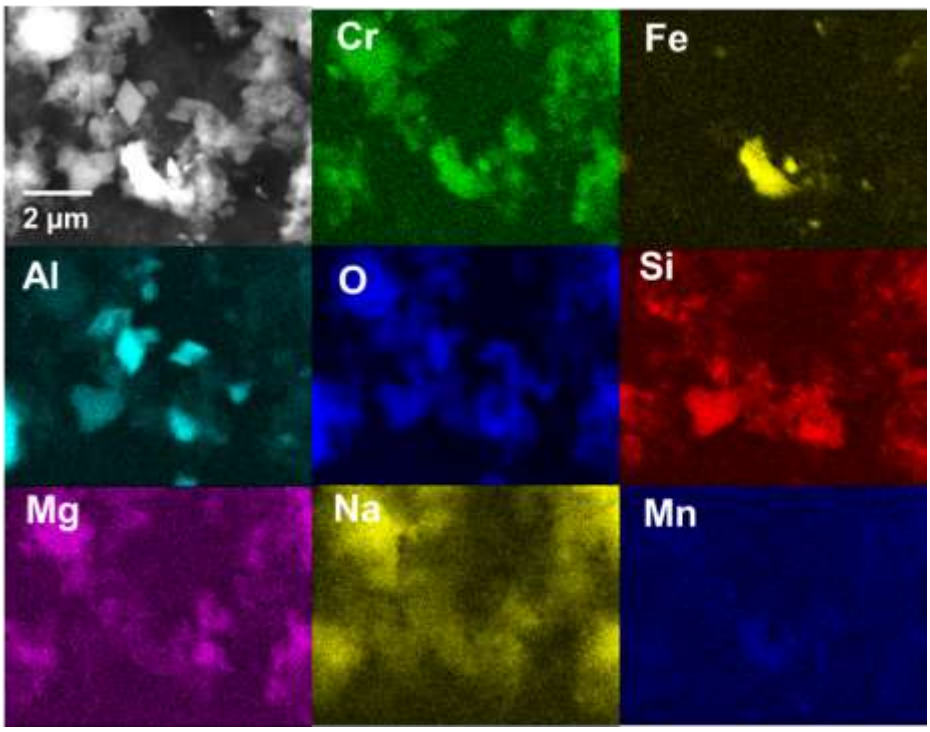

Figure 3-3 High magnification elemental maps of boehmite particles showing major elements and a BSE image of the waste sample.

Much higher magnification elemental maps of the boehmite crystals are shown in Figure 3-4 and Figure 3-5. These again show the very faint line of Si surrounding the boehmite particle.

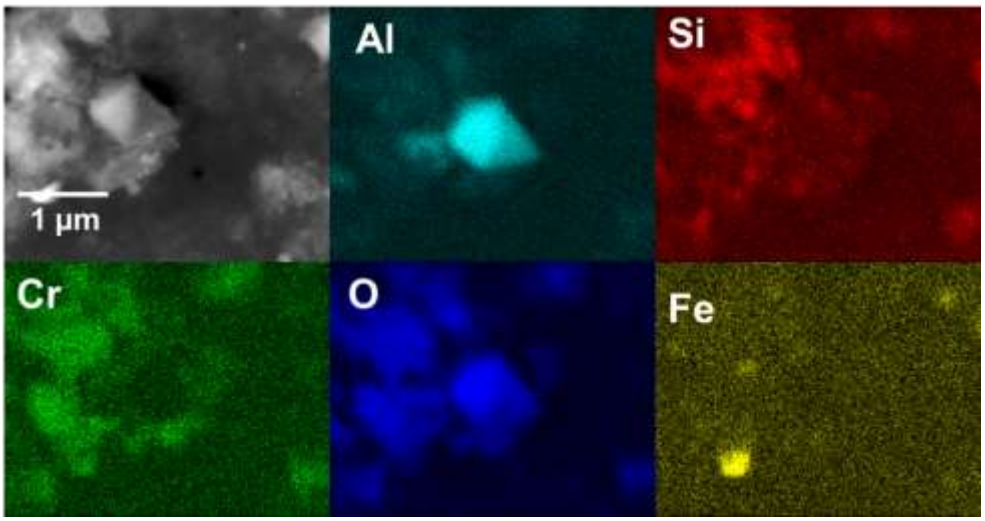

Figure 3-4 High magnification elemental maps of boehmite showing the occurrence of Al and O in the crystal, surrounded by Si and Cr, and devoid of Fe.

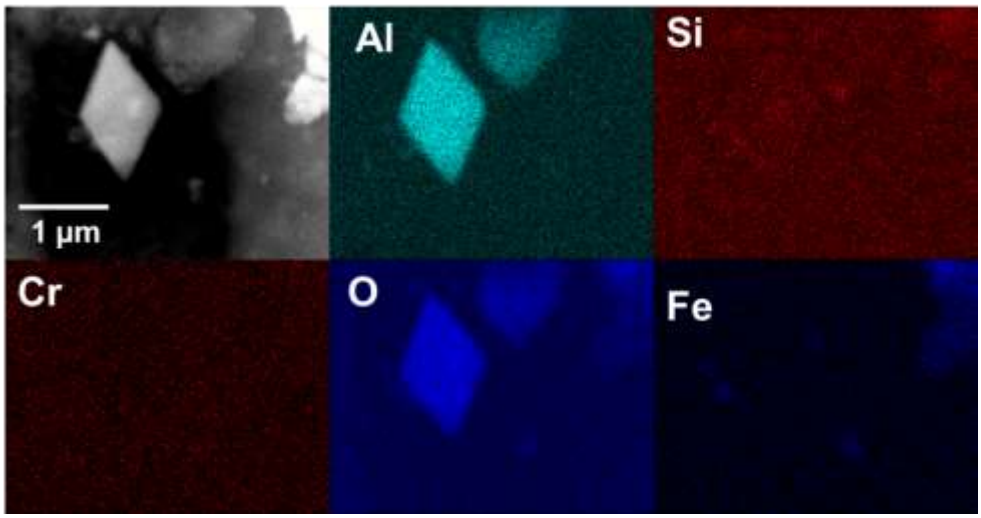

Figure 3-5 High magnification elemental maps of boehmite showing major elements and showing the encapsulation of the boehmite by Si.

4.0 Discussion

Other major phases in the waste tanks, apart from the aluminum oxides, includes sodium nitrates and carbonates, chromium oxides, the Al-silicate phase, cancrinite, as well as manganese oxides and Fe-Cr phases. The very small crystallite size for boehmite in AP-105 tank waste suggests that crystal growth was terminated, possibly by impurities that could control subsequent dissolution processes during waste treatment. According to the SEM-EDS analyses, both Cr and Si were closely associated with the boehmite. Work by Chatterjee et al. [3] has determined that it is highly unfavorable for Cr to become incorporated into boehmite. In this study, we observed the close association of Cr and boehmite but did not find evidence for incorporation. Nevertheless, the images of boehmite in AP-105 and the associated Cr phase are similar to those prepared synthetically by Chatterjee et al. and show particles of Cr-oxide attached to the (101) edges of boehmite. Other studies by Conroy et al. [4] do demonstrate that Fe can become incorporated into boehmite and that this boehmite can impact the dissolution behavior under some conditions by making the boehmite more recalcitrant. However, although Fe was common in the AP-105 waste but, at least during this SEM-EDS analysis, we found no evidence of Fe incorporation or even association. Higher resolution microscopy would clearly resolve this question. The one element that was clearly associated and attached to the edges of boehmite was Si. The EDS maps shows Si outlining boehmite crystals (see Figure 4-1 for a schematic diagram showing the arrangement of boehmite in the AP-105 waste). The exact nature of this association is unknown and would require higher resolution TEM/STEM imaging to determine the bonding characteristics. In closely related work relevant to the dissolution of boehmite, Ireland et al. [5] used TEM to show that in the presence of Ti, boehmite dissolution slows due to the formation of an inhomogeneous titanate layer on the boehmite surface. The Si layer observed in this study shares several characteristics of the Ti-layer found by Ireland et al. The Si layer outlines the (101) reactive surface and appears to be bonded to the Al-phase. It was also demonstrated that aluminum can associate with titanium and further inhibit reaction but it is unclear if similar effects would occur with the Si-layered boehmite in AP-105.

The exceedingly slow boehmite dissolution under caustic conditions has been predicted to impact the operational efficiency of the WTP at Hanford; although, direct vitrification in the DFLAW avoids this issue for the AP-105 liquid wastes. Determining the actual reasons for the slow kinetics and/or low solubility of boehmite could lead to improved processing times for sludge-types wastes, and although AP-105 has a very low concentration of boehmite and is not intended for processing at WTP, information on the composition of boehmite in this waste could be usefully applied to other waste streams.

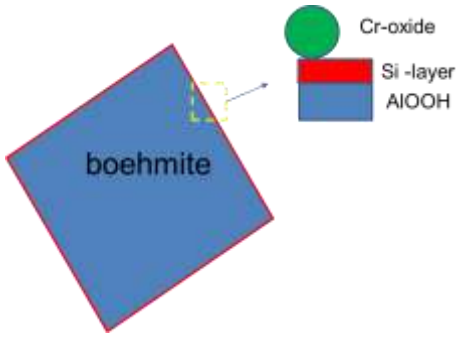

Figure 4-1 Schematic of boehmite morphology in AP-105 tank waste showing the association of Si and Cr phases with the AlOOH phase

Particle sizes were estimated from the some of the micrographs. In Figure 4-2, the Fe-particles have been placed on a log-normal plot. There is a strong divergence from the distribution. This distribution includes the large >30 um particle that was observed in Figure 4-3. Because of the nature of the overlapping particles, it was difficult to extract further information regarding particle sizes from these specimens.

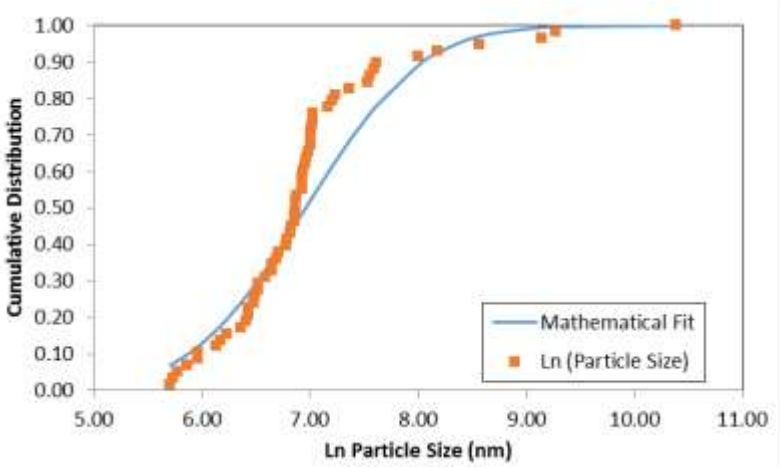

Figure 4-2 Plot showing the distribution of Fe-bearing particles with a cumulative distribution function

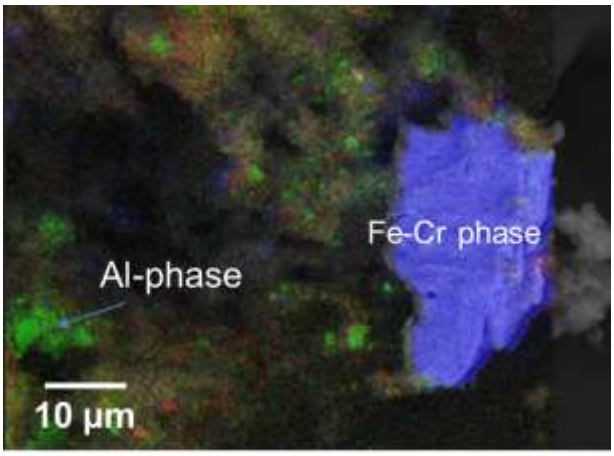

Figure 4-3 SEM image with RGB-EDS elemental map superimposed. Several different types of particles were observed in AP-105

High resolution TEM/STEM could provide the ability to address the scientific questions raised above. For example, it has been recently demonstrated that chemical composition can be analyzed under liquid condition with appropriate modification of the liquid cell. This capability will allow us to directly monitor the chemical and structural evolution under native liquid reaction processes. These innovative approaches for investigating the chemistry of nuclear related systems at the micron and nano-scale can provide new insight into dissolution and more accurate predictive tools for dissolution processes.

5.0 References

1. DeLorenzo, D. S., DiCenso, A. T., Amato, L. C., Stephens, R. H., Johnson, K. W. Report Tank Characterization Report for Double-Shell Tank 241-AP-105, WHC-SD-WM-ER-36-REV 0, September 1994.
2. Ferriter, S. D., Derivation of Best-Basis Inventory for Tank 241-AP-105 as of July 1, 2016, Washington River Protection solutions, RPP-RPT-43498, Rev 4., September 2016.
3. Chatterjee, S., Conroy, M. A., Smith, F. N., Jung, H-J, Wang, Z., Peterson, R. A., Huq, A., Burtt, D. G., Ilton, E. S., Buck, E. C., Can Cr(III) substitute for Al(III) in the structure of Boehmite? RSC Advances, 2016, 6, 107628-107637.
4. Conroy, M., Soltis, J. A., Wittman, R. S., Smith, F. N., Chatterjee, S., Zhang, X., Ilton, E. S., Buck, E. C., Importance of interlayer H bonding structure to the stability of layered minerals, Scientific Reports, 2017, 7, 13274.
5. Ireland, M., Wnag, X., Radomirovic, T., Smith, P., Jones, F., Investigating the impact of anatase on the dissolution of boehmite, Hydrometallurgy, 2014, 147–148, 246-254.

No. of Copies

No. of Copies

3 **Local Distribution**
Pacific Northwest National Laboratory

Edgar C. Buck	P7-27
David L. Blanchard	P7-27

Pacific Northwest
NATIONAL LABORATORY

U.S. DEPARTMENT OF
ENERGY

902 Battelle Boulevard
P.O. Box 999
Richland, WA 99352
1-888-375-PNNL (7665)
www.pnl.gov